INFRAMATION
THE THERMOGRAPHER'S CONFERENCE

Thermography Detection on The Fatigue Damage of Reactor Pressure Vessel (RPV) Steels

B. Yang, P.K. Liaw, D. Fielden
University of Tennessee

J.Y. Huang & R.C. Kuo
Institute of Nuclear Energy Research, Taiwan

J.G. Huang
Taiwan Power Company, Taiwan

ABSTRACT

A high-speed and high-sensitivity thermographic infrared (IR) imaging system has been used for nondestructive evaluation of temperature evolutions during fatigue testing of Reactor Pressure Vessel (RPV) steels. During each fatigue cycle, the specimen temperature was detected to oscillate within approximately 0.5ºC depending on the loading conditions and test materials. When the applied stress reached the minimum, the temperature typically approached the maximum. However, the applied maximum stress did not necessarily correspond to the minimum temperature. A theoretical framework was attempted to predict temperature evolutions based on thermoelastic and inelastic effects, and heat-conduction models. Temperature oscillation during fatigue resulted from the thermoelastic effects, while the increase in the mean temperature derived from the inelastic behavior of the materials. The predicted temperature evolutions during fatigue were found to be in good agreement with the thermographic results measured by the advanced high-speed and high-sensitivity IR camera. Furthermore, the back calculation from the observed temperature was conducted to obtain inelastic deformation and stress-strain curves during fatigue.

Keywords: infrared thermography, fatigue, thermoelastic, inelastic, temperature, non-destructive testing, NDT

INTRODUCTION

Fatigue damage analysis has been investigated intensively. For thousands of years, people have been trying to learn from the broken tools, machines, and architectures to improve their techniques and designs and avoid possible failures or extend fatigue life as much as they could. It has always been a great temptation to find a method to watch the target fatigue damage process simultaneously so that in time reparations will be possible and failures and lost can be minimized to the maximum extent. However, until today, this has been shown to be a very complex problem and we still have a long way to go. In the last hundred years, along with the substantial growth of human technologies, many nondestructive evaluation methods have been developed, such as ultrasonics, acoustic emission, eddy current, and X-ray [1-4]. However, most of these methods have their own limitations. Some methods require special sample preparations and cannot be applied in most working conditions, such as X-ray. Some methods such as ultrasonics, acoustic emission, and eddy current rely on sensors that are put on several points of the interested materials. They can only obtain information from these points and conclusions will depend on derivations and suppositions to calculate the mechanical state on other sites of the materials. These methods cannot directly “see” the fatigue damage process simultaneously.

Thermography can do this. It is a nondestructive evaluation method that can see the temperature evolution on the targets using infrared techniques. Since any mechanical damage process involves energy dissipation and heat generation, the damaged regions become visible on thermographs, often long before the failure happens. Thermography is well known for its military application to see combatant in darkness and its application in hospitals to see sick tissues with abnormal temperatures. However, its

application in mechanical processes was restrained until recently by the limited sensitivity of the available instrumentation until the last two decades, and relatively little work on thermography has been conducted to assess mechanical characteristics [5-10].

This paper describes reactor pressure vessel steels that are subjected to 10 Hz and 20 Hz fatigue tests and monitored by an infrared imaging system (IR camera) to record the temperature evolution during fatigue. Theoretical models including thermoelastic, inelastic, and heat-conduction effects are formulated to explain and predict the observed temperature variation during fatigue. Furthermore, the back calculation of thermography was conducted to predict the stress-strain behavior during fatigue, which was found to be in good agreement with the experimental results.

EXPERIMENTAL PROCEDURES

The material used in fatigue tests is a reactor pressure vessel (RPV) steel (SA533B1I2), which is composed of 0.203C, 0.23Si, 1.34Mn, < 0.02P, 0.015S, 0.50Ni, 0.53Mo, 0.15Al, 0.005N, 0.01Cu, and the balance Fe in weight percent. Fatigue test samples are cylindrical bars with a gage length of 1.27 cm and a diameter of 0.508 cm at the gage section. For the 20 Hz fatigue experiments in air, the specimens were loaded on a MTS (Material Test System) machine (Model 810) at R = 0.2, where R = □min/□max, □min and □max are the applied minimum and maximum stresses, respectively. A load control mode was used, and different maximum stress levels ranging from 500 MPa to 650 MPa were applied.

A Raytheon Galileo thermographic IR imaging system was used with a 320 x 256 pixel focal-plane-array InSb detector that is sensitive to 3 to 5 mm thermal radiation. The temperature sensitivity of the IR camera is 0.015ºC at 23ºC. The spatial resolution of the system is equal to 5.4 μm, when a microscope attachment is used. High-speed data acquisition capabilities are available at 128 Hz with a full frame, and 50,000 Hz with a narrow window. During fatigue testing, a thin sub-micron graphite coating was applied on the gage-length section of the fatigue sample to decrease IR reflections. A fully-automated software system was employed to acquire temperature distributions of the test samples during fatigue experiments.

A thermocouple was attached to the sample to calibrate the IR camera at the beginning of each test. During calibration, a heat gun was used to heat up the specimen to a given temperature, and then the specimen was cooled in air. Different temperatures were read from the thermocouple during cooling. The calibrated intensities of the IR camera were used to generate temperature maps. The IR cameras were used in the range of 0.1 Hz to 120 Hz. To capture the detailed thermoelastic effect during 20 Hz fatigue tests, the IR camera was employed at a high speed of 120 Hz.

RESULTS AND DISCUSSION

Figure 1 shows the temperature profile of a RPV steel specimen during 20 Hz fatigue testing with a R ratio of 0.2 and maximum stress level of 640 MPa. The temperature profile was recorded at the midpoint of the specimen gage-length section using the IR camera at a high speed of 120 Hz. In Figure 1, an initial increase in the temperature from 23.7ºC to 28.5ºC, followed by a temperature decrease (i.e., a temperature hump) in the first 100 cycles, was observed. After the hump, the temperature approached a steady-state of about 27°C due to the thermal equilibrium between the specimen and the environment. Next, the temperature increased abruptly from approximately 27°C to 46°C until the specimen broke due to the heat from the large plastic deformation at the crack tip. Following that, the sample failed, and the temperature dropped.

A more detailed observation of the temperature hump is shown as the dashed line in Figure 2. A slight temperature decrease before fatigue cycling at the ramp-up period of the machine was observed due to the thermoelastic effect. Then, there is a rapid temperature increase from the first fatigue cycle at about 0.7 seconds, and reached a maximum at about 2 seconds. After that, the temperature decreased gradually to a relatively constant value. However, if the test is stopped after the temperature becomes stable, and then restarted, no temperature hump was observed. The corresponding results were plotted

as the solid line in Figure 2. At the same time, temperature oscillations within the range of approximately less than 0.6°C were found within each fatigue cycle in both tests indicated by the dashed and solid lines.

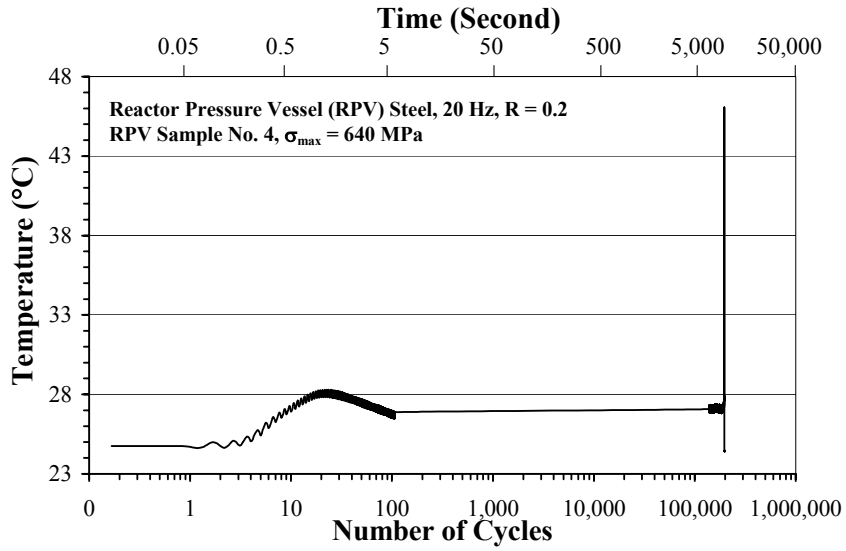

Figure 1. *Temperature Evolution of Reactor Pressure Vessel Steel High-cycle, Fatigue-tested at 20 Hz, Taken at a High IR Camera Speed of 120 Hz.115*

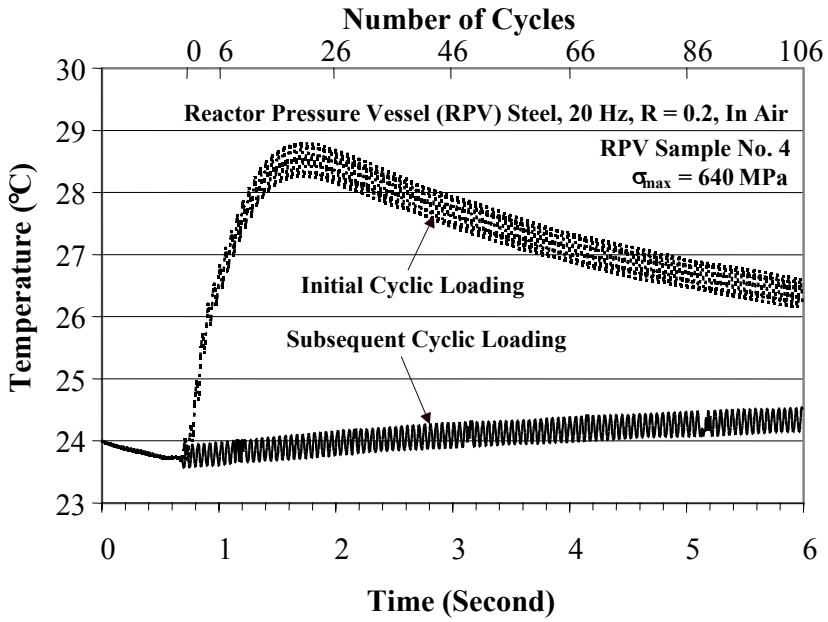

Figure 2. *Temperature Evolutions of Reactor Pressure Vessel Steel High-cycle, Fatigue-tested at 20 Hz, s_{max} = 640 MPa, Taken at a High IR Camera Speed of 120 Hz.*

A reasonable explanation of the presence of the temperature hump can be obtained from the stress-strain curve in Figure 3. This is a typical stress-strain curve for the tension-tension fatigue test. Corresponding to the temperature rise from 0.7 seconds to 2.0 seconds in Figure 2, the stress-strain curve in Figure 3

moves from the first cycle to 26 cycles, and the plastic strain increases from 0 to nearly a saturated value of 5%. During this period of time, a great amount of heat is generated from the large plastic deformation, and the temperature of the sample increases quickly. Moreover, the yielding phenomenon of RPV steel is observed in the monotonic tensile test, which contributes to the initial large plastic strain for the first several cycles, and, in turn, more heat is generated. For materials without a yielding phenomenon, the plastic strain is expected to decrease during each fatigue cycle due to the tensile hardening effect. On the contrary, the hysteresis loops of RPV steel during fatigue testing were observed to increase during the initial 1-2% plastic deformation, which corresponds to the yielding phenomenon.

The explanation of the yielding phenomenon arises originally from the idea that the dislocation sources are locked or pined by the solute atom interactions. According to this explanation, at the beginning of the test, when the stress is higher than the yielding stress, dislocations are pulled free from the interactions with the solute-atoms (carbon or nitrogen) atmosphere. Slip can then occur at a lower stress, and in this way, larger plastic deformation is expected. However, after that, very little plastic stain occurs due to the strain-hardening effect, and the temperature decreases when the heat inside the sample is conducted to the environment, and finally reaches a relatively constant value due to the heat equilibrium between the heat generation of the specimen subjected to cyclic loading and the environment.

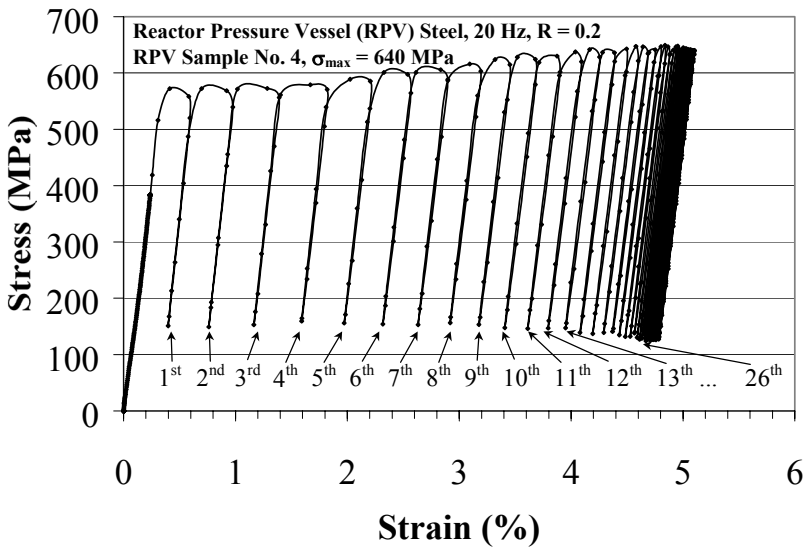

Figure 3: *Stress versus Strain Results of Reactor Pressure Vessel Steel High-cycle, Fatigue-tested at 20 Hz, smax = 640 MPa.*

Then, if the fatigue test is terminated and restarted, since the plastic strain has already saturated, little heat will be generated resulting from the plastic deformation. Thus, there will be no rapid temperature rise in the first 100 cycles in the solid line presented in Figure 2.

Now, the next question is: can we quantify the fatigue damage from the temperature changes we observed? To answer this question, it is important to clarify the relationship between temperature and stress-strain state first. The material temperature evolution during mechanical process without an outside heat source can be affected by (I) the thermoelastic, (II) the inelastic, and (III) the heat-transfer effects. The thermoelastic effect relates the temperature with the stress and elastic strain [11, 12], the inelastic effect uncovers the relationship between the temperature and plastic deformation [13, 14], and the heat-transfer effects change the material temperature by heat exchanges with environment.

As an example, Figure 4 provides a close observation of the relationship among the stress, strain, and temperature at the beginning stage of a fatigue cycling of the RPV steel. When the stress begins to fluctuate in a sinusoidal wave, the mean strain rises up, while the strain amplitude remains the same. The

temperature also fluctuates with the stress, and the mean temperature increases. Lines, A1, A3, and A5, represent the time when the applied stress increases to the yielding point, while lines, A2, A4, and A6, show the time when the stress decreases to the yielding point. Lines, B1, B2, and B3, correspond to the time when each of the stress cycles reaches the highest point, and lines, C1 and C2, to the lowest point. It shows that when the stress reaches the lowest value, the strain also approaches the lowest value (lines, C1 and C2), and the temperature rises to the highest point. Since this stress value is much lower than the yielding strength, the observed experimental results match the elastic stress-strain relation and the thermoelastic effect quite well, i.e., decreasing the stress increases the temperature, as reported later.

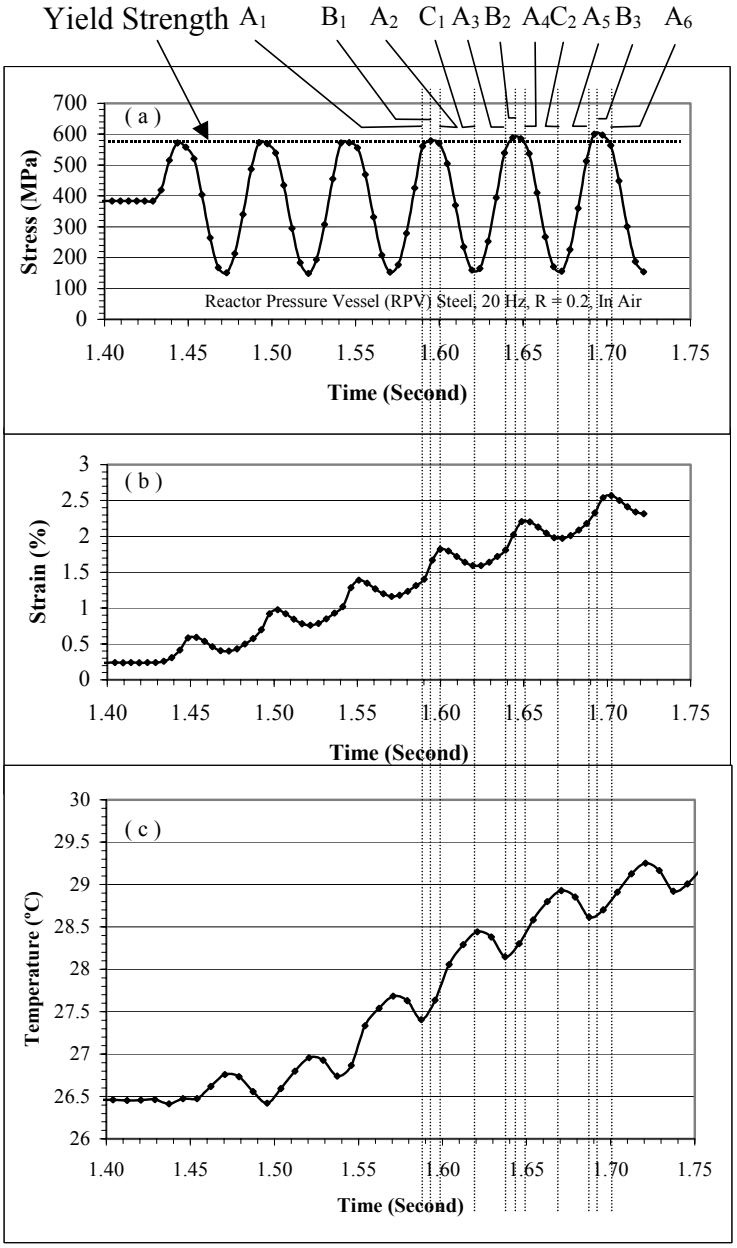

Figure 4. *Stress-Strain-Temperature versus Time Results of Reactor Pressure Vessel Steel during Initial Fatigue Cycling at 20 Hz, σ_{max} = 640 MPa, Taken at an IR Camera Speed of 120 Hz [(a) Stress versus Time, (b) Strain versus Time, and (c) Temperature versus Time*

However, if Figure 3 is examined carefully, there is a phase difference among the stress, strain, and temperature profiles for lines, B1, B2, and B3, which correspond to the highest stresses in the fatigue

cycles. The highest value for the strain seems to occur somewhat later than that for the stress, and the lowest point of the temperature appears earlier than the highest stress value. This trend results from the fact that at this time, the stress has already passed the yielding point, and the effect of the plastic deformation should be considered. For the strain, even after the stress passes the highest value, the plastic strain is still increasing due to the yield-point phenomenon, which results in large strains. This process continues until the stress drops lower than the yielding point. This is why the highest point for the strain appears later than that for the maximum stress. Lines, A2, A4, and A6, correspond to the unloading period when the stress decreases to the yielding point, and the strain reaches the maximum value of each fatigue cycle, since below the yielding strength, the generation of the plastic strain is insignificant.

On the other hand, the mean temperature will rise up, when the stress reaches the yielding point because of the plastic deformation and yield-point phenomenon. Thus, the lowest value of the temperature appears earlier than the highest value of the stress, which exceeds the yield strength. Lines, A1, A3, and A5, in Figure 4 show that the lowest temperature points appear when the stress approaches the yielding point, which induces the plastic strain, and starts to increase the temperature.

THEORETICAL MODELING

Based on the knowledge above, a one-dimensional model combining the thermoelastic, inelastic, and heat-transfer effects will be formulated in the following and the relationship among the stress, strain, and temperature will be quantified. Forward calculation will be tried to predict the temperature evolution process from the stress-strain data of the fatigue testing. Specifically, the temperature evolution during fatigue will be simulated cycle by cycle using this model and compared with the experimental data. Then backward calculation will be implemented to predict the stress-strain curve, which shows the mechanical damage process during fatigue, from the temperature data obtained by the thermography technique.

Thermoelastic Effect

The basic relationship among the entropy, temperature, and energy can be derived from the law of thermodynamics in the form [11, 12]:

$$ds = \frac{1}{T}\frac{\partial U}{\partial T}dT - \sum^{ij}\frac{\partial \sigma_{ij}}{\partial T}d\varepsilon_{ij}\text{ , i, j = 1, 2, 3} \tag{1}$$

where

s = entropy
U = internal energy
T = absolute temperature
σ_{ij} = stress component, and
ε_{ij} = strain component

Considering $\frac{\partial U}{\partial T} = \frac{\partial Q}{\partial T} = C_\varepsilon \rho$, and using the equations

$\sigma_{ij} = 2G(\varepsilon_{ij} + \frac{\nu}{1-2\nu}e\delta_{ij} - \frac{1+\nu}{1-2\nu}\alpha\Delta T\delta_{ij})$ and $E = 2G(1+\nu)$,

the following equation can be derived:

$$ds = C_\varepsilon \rho\frac{dT}{T} + \frac{\alpha E}{1-2\nu}(d\varepsilon_1 + d\varepsilon_2 + d\varepsilon_3) \tag{2}$$

where

Q = outside heat source
ρ = density
ΔT = temperature change
G = shear modulus
ν = Poisson's ratio
$e = \varepsilon_1 + \varepsilon_2 + \varepsilon_3$
E = Young's modulus
α = coefficient of linear expansion
$\delta_{ij} = \langle 1(i=j) | 0(i \neq j) \rangle$, and
C_ε = heat capacity at a constant strain

With small changes in temperature, integrating Equation (2):

$$s = \frac{C_\varepsilon \rho \Delta T}{T} + \frac{\alpha E}{1-2\nu}(\varepsilon_1 + \varepsilon_2 + \varepsilon_3) \tag{3}$$

At a constant pressure, using a stress tensor to replace the strain tensor, and considering $C_p - C_\varepsilon = \frac{3E\alpha^2 T}{\rho(1-2\upsilon)}$, Equation (3) becomes:

$$Q = C_p \rho \Delta T + T\alpha(\sigma_1 + \sigma_2 + \sigma_3) \tag{4}$$

where

C_p = heat capacity at a constant pressure.

Under adiabatic conditions, $Q = 0$,

$$\Delta T = -\frac{T\alpha}{C_p \rho}(\sigma_1 + \sigma_2 + \sigma_3) \tag{5}$$

The above equation can be written in the form of

$$\Delta T = -KT(\sigma_1 + \sigma_2 + \sigma_3) \tag{6}$$

where $K = \frac{\alpha}{C_p \rho}$.

While the absolute temperature of the material does not change sharply during each fatigue cycle, the temperature will fluctuate proportional to the sum of the principal stresses. While the stress increases, the temperature will decrease and vice versa [Equation (6)]. Experimentally, during fatigue, it was observed that the temperature of the specimen decreases, proportional to the increase of the stress in the ramp-up period of the MTS machine, and oscillates regularly during each fatigue cycles (Figures 4). These trends can be attributed to the thermoelastic effect, as described above.

Inelastic Effect

The mean temperature rise in Figure 4 can be attributed to the heat from the plastic deformation, which can also be called the inelastic effect. To quantify the inelastic effect in fatigue cycling, the following assumptions need to be made:

Consider an isotropic, long, and slender bar, which is subjected to a homogeneously-applied deformation field such that the resulting stress field is everywhere uniaxial in one dimension.

Only a fixed system of one-dimensional axis, *x*, will be considered.

Thus, considering the inelastic effect, the basic thermodynamic equation [13, 14] is:

$$\rho C_p \frac{\partial T(x,t)}{\partial t} = Q' \tag{7}$$

where

Q' = heat generated inside the material.

Since $W = \int Q' dt = \int \sigma d\varepsilon$, integrating Equation (7) with time gives:

$$\rho C_p \theta_i = \int_{\varepsilon_1}^{\varepsilon_2} \sigma_u d\varepsilon - \int_{\varepsilon_1}^{\varepsilon_2} \sigma_l d\varepsilon = A_i \tag{8}$$

where

θ = temperature change due to the thermoplastic effect for each fatigue cycle

ε_1 = minimum strain of the hysteresis loop

ε_2 = maximum strain of the hysteresis loop

σ_u = stress in the upper part of the hysteresis loop

σ_l = stress in the lower part of the hysteresis loop

A = area for each hysteresis loop, and

i = number for each fatigue cycle

Heat-Conduction Effect

To provide a better prediction of the thermography results, the heat-transfer effect needs to be considered. For RPV steels tested in air, two heat-transfer processes are involved. One is the heat conduction between the specimen and the main body of the MTS machine through grips, and the other is the heat transfer between the specimen and the air around it. However, comparing with the large heat capacity in steels, neglecting the heat transfer with air will be reasonable.

The equation for heat conduction in solids with a constant thermal conductivity is:

$$\rho C_p \frac{\partial T}{\partial t} = k\left(\frac{\partial^2 T}{\partial x^2} + \frac{\partial^2 T}{\partial y^2} + \frac{\partial^2 T}{\partial z^2}\right) + q \tag{9}$$

where

k = thermal conductivity of the material, and
q = energy conversion rate per unit volume.
For a steady one-dimensional conduction without energy conversion, Equation (9) becomes:

$$\rho C_p \frac{\partial T}{\partial t} = k \frac{\partial^2 T}{\partial x^2} \tag{10}$$

The specimen is held by a pair of grips that are loaded on the machine. For the continuity of the one-dimensional heat-conduction model, the length of the grips and non-gage section of the specimen need to be converted into an effective length of material with the same cross-sectional area as the gage section. The key is that the heat passing through a cross section should be the same before and after conversion. As for the inclusion of the heat-conduction effect, the temperature in the main body of the machine is equal to room temperature, and the length of the grips (20.32 cm) and non-gage length of the specimen (3.83 cm) are converted into an effective length of 14.05 cm with a diameter of 5.1 cm (the same as the gage diameter of the specimen). Combining with the real gage length (1.27 cm), the total effective length will be 15.32 cm. Considering that the specimen is a homogeneous round bar, and assuming that the temperature gradient is constant with the *x*-axis, a simplification can be made as follow:

$$\frac{\partial T}{\partial x} = \frac{T - T_0}{\Delta x} \tag{11}$$

where

T_0 = room temperature, and
Δx = effective length of 15.32 cm from the center of the specimen to the end of the grip.

Since:

$$k \frac{\partial T^2}{\partial x^2} = k \frac{\partial (\frac{T - T_0}{\Delta x})}{\partial x} = k \frac{1}{\Delta x} \frac{\partial T}{\partial x} \tag{12}$$

Equation (10) can be converted into:

$$\rho C_p \frac{\partial T}{\partial t} = k \frac{1}{\Delta x} \frac{\partial T}{\partial x} \tag{13}$$

The heat-conduction rate can then be determined by equation (14):

$$\frac{\partial T}{\partial t} = k \frac{1}{(\Delta x)^2 \rho C_p} (T - T_0) \tag{14}$$

FORWARD CALCULATIONS

In this section, the thermoelastic, thermodynamic, and heat-transfer effects are combined to predict the temperature evolution versus number of cycles curves. The temperature evolutions will be predicted using the stress and strain results during fatigue, and compared with the experimental data.

The relevant material constants of the present RPV steel are:

a) Linear thermal expansion coefficient: $\alpha = 1.1 \times 10^{-5}$ /°C

b) Density: $\rho = 7.8\ \text{g/cm}^3$

c) Specific heat at a constant pressure: $C_p = 0.48\ \text{J/g°C}$

In uniaxial fatigue testing, considering the uniaxial-stress condition, there is only one principal stress, σ_1. Thus, Equation (6) can then be simplified to:

$$\Delta T = -KT\sigma_1 \tag{15}$$

The temperature evolution due to the thermoelastic effect can be calculated by Equation (15). Figure 5 shows the predicted temperature oscillation during the first 18 fatigue cycles. The zero point of ΔT corresponds to the initial temperature when the stress is at the mean stress level. A slight decrease of the minimum temperature during each fatigue cycle was observed due to the increase of the corresponding maximum stress with each fatigue cycle during the initial cycling of the MTS machine, which has been explained before.

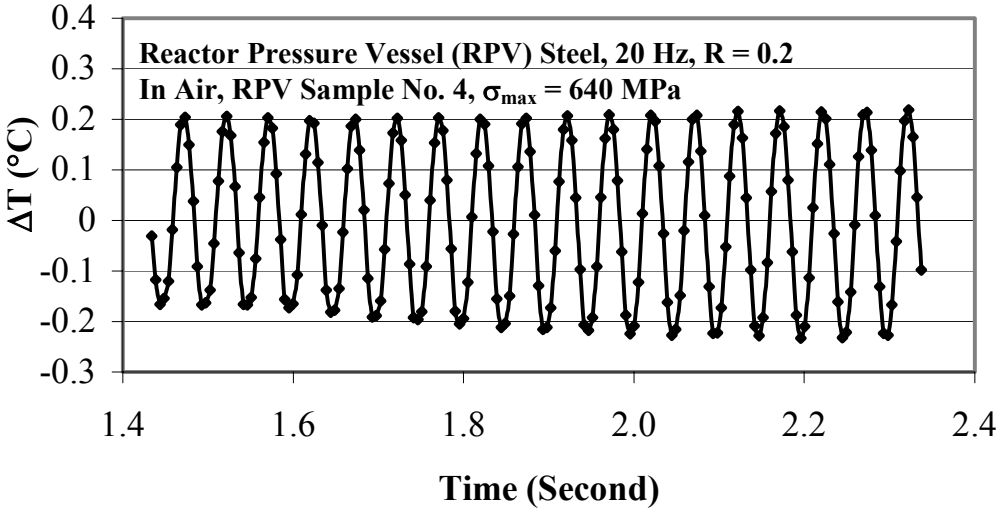

Figure 5. *Predicted Temperature Oscillation of Reactor Pressure Vessel Steel during the First 18 Cycles of Fatigue Testing at 20 Hz, σ_{max} = 640 MPa.*

Using the stress-strain data that was recorded during fatigue testing to calculate the area of each hysteresis loop, the mean temperature change due to the inelastic effect can be predicted from Equation (8). Figure 6 represents the predicted change of the mean temperature resulted from the plastic deformation during the first 18 fatigue cycles. Due to the fact that plastic deformation takes place only when the applied stress is greater than the yielding point, which is a small portion of each cycle, the mean temperature will only increase in this portion of each cycle, and thus, a stair shape of the mean temperature versus time curve is expected in Figure 6.

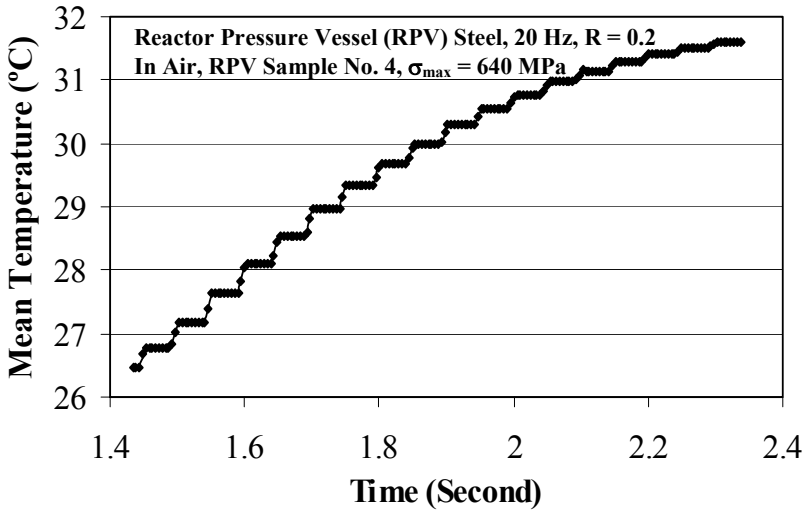

Figure 6. *Predicted Mean Temperature Change of Reactor Pressure Vessel Steel during the First 18 Cycles of Fatigue Testing at 20 Hz, σ_{max} = 640 MPa.*

For each data point recorded in the fatigue test at 20 Hz, the time interval, Δt, is 0.00483 seconds. If considering $dt \approx \Delta t$ = 0.00483s, Equation (14) becomes:

$$dT_j = k\frac{1}{(\Delta x)^2 \rho C_p}(T_j - T_0)dt \tag{16}$$

where

j = number of the fatigue data point, and
dT_j = temperature correction due to the heat-conduction effect for each fatigue data point

Using Equation (16) to refine the temperature calculation, the temperature change for each data point becomes:

$$\Delta T_{jc} = \Delta T_j - \sum_{n=1}^{j} dT_n \tag{17}$$

where

ΔT_{jc} = temperature change for each data point after the heat-conduction correction

ΔT_j = temperature change for each data point before the heat-conduction correction, and

$\sum_{n=1}^{i} dT_n$ = accumulation of the heat-conduction effect.

Thus, the predicted temperature for each data point after the heat-conduction correction can be written in the equation (18):

$$T_{jc} = T_0 + \Delta T_{jc} \tag{18}$$

where

T_{jc} = predicted temperature for each data point after the heat-conduction correction, and

T_0 = room temperature

Combining the calculation of the thermoelastic, inelastic, and heat-transfer effects, the theoretical temperature profile of the first 18 fatigue cycles is predicted in Figure 7. The theoretical predictions are found to be in good agreement with the experimental data. However, for the first two fatigue cycles, the predicted and measured results fail to fit each other closely, which can be explained as follows. The surface and the center of the sample have not reached a uniform thermodynamic state at the very beginning of the test. The surface temperature can be more easily dissipated, relative to the interior of the sample. Thus, the measured surface temperatures of the test specimen by thermography can be lower than the predicted values.

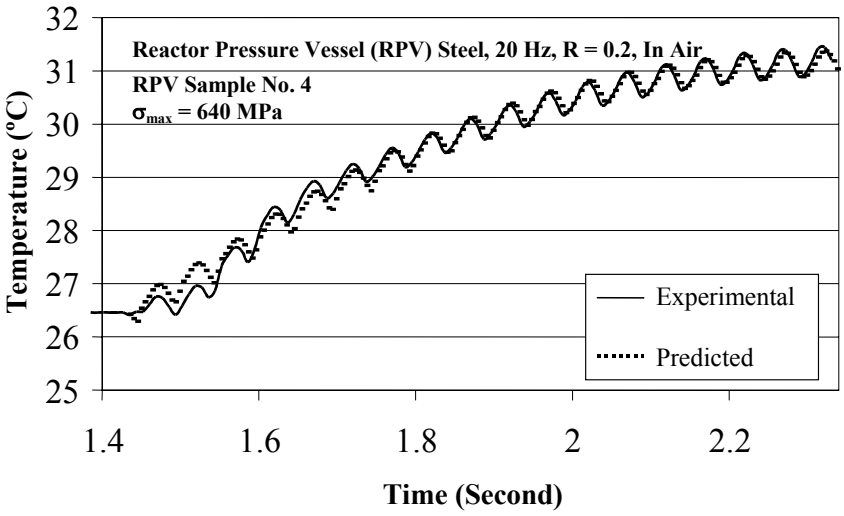

Figure 7. *Measured and Predicted Temperature Evolutions of Reactor Pressure Vessel Steel during First 18 Cycles of Fatigue Testing at 20 Hz, σ_{max} = 640 MPa.*

BACK CALCULATION

In the previous section, the prediction of the specimen temperature evolutions during fatigue has been conducted using the stress-strain data. At the same time, the mechanical behavior can also be investigated from the original temperature profile. In this section, the back calculation from the measured temperature to predict the stress and strain state during fatigue will be performed.

From the specimen temperature evolution, we can easily calculate the stress state by the thermoelastic effect. At the ramp-up period of fatigue testing, the stress goes from zero to the mean stress. At the same time, the normalized temperature goes down from 24 to 23.665°C. The mean stress can then be calculated by Equation (6) as:

$$\left(\frac{\sigma_{\min}+\sigma_{\max}}{2}\right)=\left(\frac{(23.665-24)}{-KT_0}\right) \tag{19}$$

At the constant temperature region, a temperature oscillation (ΔT_{osci}) of 0.46°C can also be expressed by equation (20):

$$\Delta T_{osci} = -KT(\sigma_{\max} - \sigma_{\min}) \tag{20}$$

Thus,

$$\left(\frac{\sigma_{\max} - \sigma_{\min}}{2}\right) = \frac{\Delta T_{osci}}{-2KT} \tag{21}$$

Using Equations (19) and (21), the minimum and maximum stresses were then calculated as 123 MPa and 638 MPa, respectively, which are very close to the nominal stress levels in the test (σ_{min} = 123 MPa and σ_{max} = 640 MPa). The elastic strain, ε_e, in fatigue testing can then be calculated easily by the equation:

$$\varepsilon_e = \sigma / E \tag{22}$$

However, the inelastic strain of the specimen cannot be directly obtained from the original temperature evolution because the mean temperature change is determined not only by the inelastic effect but also by the heat-conduction effect. Thus, the first step to calculate the inelastic strain will be the back calculation to exclude the heat-conduction effect from the original temperature evolution.

The equation that is used for the back calculation is the same as Equation (14):

$$dT_j = k\frac{1}{\Delta x^2 \rho C_p}(T_j - T_0)dt \tag{23}$$

where

j = the jth experimental temperature data point.

Using Equation (23) to eliminate the heat-conduction effect from the original temperature evolution, the temperature for each data point becomes:

$$T_{jc} = T_j + \sum_{n=1}^{j} dT_n \tag{24}$$

where

T_{jc} = temperature after the back calculation by excluding the heat-conduction effect.

A way in calculating the inelastic strain for each fatigue data point can be obtained by excluding the thermoelastic effect from the temperature-evolution through back calculation. The corresponding equation is shown below:

$$T'_{jc} = T_{jc} + KT_{jc}\sigma \tag{25}$$

where

T'_{jc} = temperature after the back calculation by excluding both the heat-conduction effect and the thermoelastic effect.

Figure 8 represents the back-calculated temperature evolutions excluding the heat-conduction and thermoelastic effects. The solid line shows the temperature evolution excluding the heat-conduction and the thermoelastic effects using Equations (24) and (25), the long dash line exhibits the temperature profile excluding the heat-conduction effect using Equation (24) and including the thermoelastic effect. Comparing these two curves shows that the solid line is higher than the short dash line because of the fact that the thermoelastic effect always intends to decrease the temperature in a tension-tension test. A

close observation of the solid line shows that temperature fluctuation cannot be 100% eliminated during each fatigue cycle, which is due to the simplification in the thermoelastic equation.

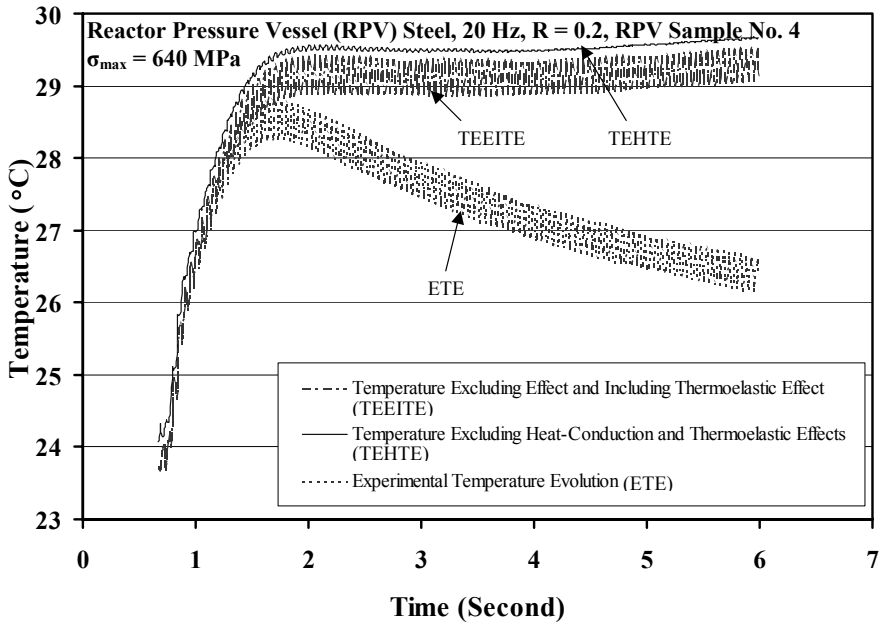

Figure 8. *Back-Calculated Temperature Evolutions Excluding Heat-conduction and Thermoelastic Effects of Reactor Pressure Vessel Steel Tested at 20 Hz, σ_{max} = 640 MPa.*

After the elimination of the thermoelastic effect, the inelastic strain can be calculated by equation (26):

$$\varepsilon_{in_j} = \frac{\rho C_p (T'_{(j+1)c} - T'_{jc})}{\sigma_{\max}} \tag{26}$$

where

ε_{in_j} = calculated inelastic strain for the j_{th} data point

The prediction of the inelastic strain cycle by cycle has been shown to be quite accurate even after inelastic strain saturated. On the other hand, the prediction of the inelastic strain data by data depends on the elimination of the thermoelastic effect, which is difficult to be perfect. Thus, the deviation occurs when the inelastic strain decreases to nearly zero, and the number of cycles is large. However, this method provides a way to predict the evolution of the real hysteresis loops.

Combining the calculated stress, elastic strain, and inelastic strain, the predicted stress versus strain curve is shown in Figure 9. The solid line is the experimental stress versus strain curve, while the dashed line is the predicted one. Comparing the two curves shows that, after 10 cycles, the predicted data fits the experimental result quite well. However, after thousands of cycles, the plastic strain of the predicted curve does not converge to the same upper limit as the experimental one, which is due to the accumulation of the small errors induced by the residual temperature fluctuation, represented by a solid line, during each fatigue cycle (Figure 8). The inelastic strain calculated from the residual temperature fluctuation could not totally cancel out because of the limited number of data points taken during each cycle. These errors can be neglected while the inelastic strain is obvious. However, the errors will cause problems when the inelastic strain is close to zero, and the number of cycles is large.

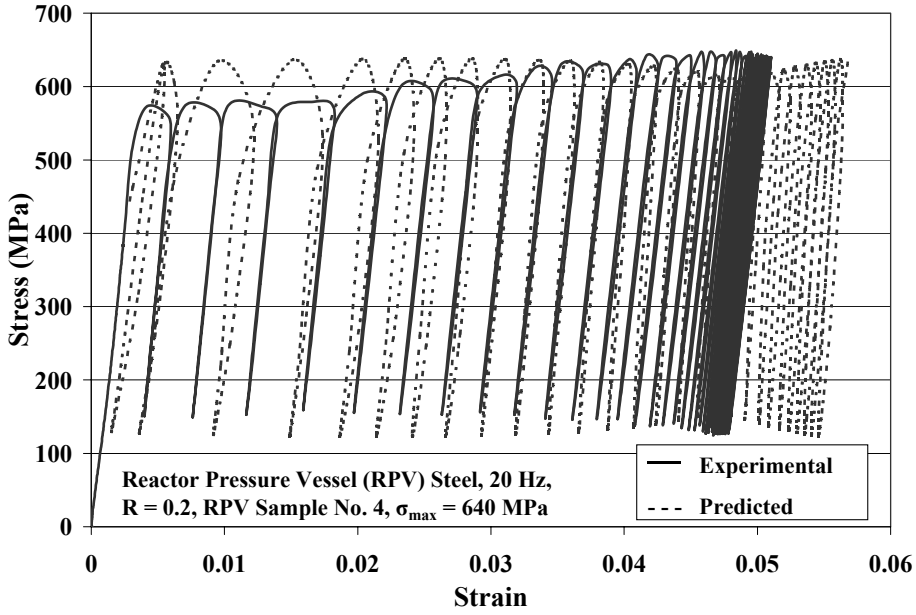

Figure 9. *Experimental and Predicted Stress versus Strain Results of Reactor Pressure Vessel Steel Tested at 20 Hz, σ_{max} = 640 MPa.*

CONCLUSIONS

In this paper, the relationship between temperature and fatigue damage has been discussed. Without outside heat sources, it can be affected by three factors: (I) the thermoelastic effect, (II) the inelastic effect, (III) heat conduction effect. Among them, the thermoelastic effect mainly contributes to the specimen temperature oscillation during each fatigue cycle while the other two effects dominate the mean temperature change of the specimen. A theoretical model has been formulated to predict the temperature profiles during fatigue testing and back calculate the stress and strain from the specimen temperature evolution. The model described in this paper is one-dimensional and it provides a way to quantify the stress-strain state and fatigue damaging from the temperature observed on the specimen simultaneously. The same model can be expanded to two dimensions and three dimensions using numerical methods, which is currently undertaken by the author. Thermography, as a new nondestructive evaluation method in mechanical process, has demonstrated its potential to “watch” the mechanical damage processes as well as to evaluate them quantitatively.

ACKNOWLEDGEMENT

Taiwan Power Company provided the major funding for this research project. It is also gratefully acknowledged regarding the financial support from the National Science Foundation (NSF), the Division of Design, Manufacture, and Industrial Innovation, under Grant No. DMI-9724476, the Combined Research-Curriculum Development (CRCD) Program, under EEC-9527527, and the Integrative Graduate Education and Research Training (IGERT) Program, under DGE-9987548, to the University of Tennessee (UT), Knoxville. This research was also financially supported by the Office of Transportation Technologies, as part of the High Temperature Materials Laboratory User Program under contract DE-AC05-96OR22464, managed by Lockheed Martin Energy Research Corporation. In addition, appreciation goes to the financial support of the Institute of Nuclear Energy Research, Taiwan, Oak Ridge National Laboratory, and Southeastern Universities Research Association.

REFERENCES

1. L. Jiang, M. Huang, C. R. Brooks, and P. K. Liaw, "Nondestructive Evaluation (NDE) and Materials Properties IV", TMS, P. K. Liaw, R. J. Arsenault, R. E. Green, Jr., K. L. Murty, and R. B. Thompson, eds., 1999, pp. 43-60.
2. M. E. Fine, Z. M. Connor, and J. D. Achenbach, "Nondestructive Evaluation (NDE) and Materials Properties IV", TMS, P. K. Liaw, R. J. Arsenault, R. E. Green, Jr., K. L. Murty, and R. B. Thompson, eds., 1999, pp. 1-9.
3. G. Birnbaum and G. Free, Eddy-current characterization of materials and structures: a symposium/sponsored by ASTM Committee E-7 on Nondestructive Testing, American Society for Testing and Materials, Gaithersburg, Md., 5-7 Sept. 1979.
4. A. A. Moss and H. I. Goldberg, Computed tomography, ultrasound and x-ray: an integrated approach, Masson Publication, USA, 1979.
5. E. G. Henneke, K. L. Reifsnider, and W. W. Strinchcomb, "Thermography – An NDI Method for Damage Detection", J. Metals, 31, 1979, pp. 11-15.
6. R. H. Blanc and E. Giacometti, "Infrared Radiometry Study of the Thermomechanical Behavior of Materials and Structures", Paper presented at the First International Conference of Stress Analysis by Thermoelastic Technics, Sira Ltd, London, November 1984.
7. B. Nayroles, R. Bouc, H. Caumon, J. C. Chezeaux, and E. Giacometti, "Telethermographie Infrarouge et Mecanique des Structures", Int. J. Eng. Sci., 19, 1981, pp. 929 – 947.
8. D. T. Lohr, N. F. Enke, and B. I. Sandor, "Analysis of Fatigue Damage Evolution by Differential Infrared Thermography", Dynamic Failure: Proceedings of the 1987 SEM Fall Conference, October 25-27, 1987, Savannah, Georgia, pp. 169-174.
9. P. K. Liaw, H. Wang, L. Jiang, B. Yang, J. Y. Huang, R. C. Kuo, and J. G. Huang, Scripta Materialia, Vol. 42, 2000, pp. 389-395.
10. M. P. Luong, Revue De Metallurgie-Cahiers D Informations Techniques, Vol. 92, Iss (2), 1995, pp. 203-212.
11. M. A. Biot, J. Appl. Phys., 27(3), March 1956, pp. 240-253.
12. R. Rocca, and M. B. Bever, Trans. Am. Inst. Mech. Eng., 188, February 1950, pp. 327-333.
13. O. W. Dillon, Journal of Mechanics and Physics in Solids, Vol. 11, 1963, pp. 21-23.
14. J. Kratochvil and O. W. Dillon, Journal of Applied Physics, Vol. 40, No. 8, 1969, pp. 3207-3218.
15. L. Jiang, H. Wang, P. K. Liaw, C. R. Brooks, and D. L. Klarstrom, "Characterization of the temperature evolution during high-cycle fatigue of the ULTIMET superalloy: Experiment and theoretical modeling", Metallurgical and Materials Transaction A, 32(9), September 2001, pp. 2279-2296.
16. H. Wang, L. Jiang, P. K. Liaw, C. R. Brooks, and D. L. Klasstrom, Metallurgical and Materials Transaction A, Vol. 31, 2000, pp. 1307-1310.
17. B. Yang, P. K. Liaw, H. Wang, L. Jiang, J. Y. Huang, R. C. Kuo, and J. G. Huang, "Thermographic Investigation of The Fatigue Behavior of Reactor Pressure Vessel Steels", Materials Science and Engineering A314, 2001, pp. 131-139.